Journal of Membrane Science 514 (2016) 125–134

Contents lists available at ScienceDirect

Journal of Membrane Science

journal homepage: www.elsevier.com/locate/memsci

Bicarbonate and chloride anion transport in anion exchange membranes ☆

Alina Amel [a], Nir Gavish [b], Liang Zhu [c], Dario R. Dekel [d,e], Michael A. Hickner [c], Yair Ein-Eli [a,e,*]

[a] Department of Materials Science and Engineering, Technion, Israel Institute of Technology, Haifa 3200003 Israel
[b] Department Mathematics, Technion, Israel Institute of Technology, Haifa 3200003 Israel
[c] Department of Materials Science and Engineering, The Pennsylvania State University, University Park, PA 16802, United States
[d] The Wolfson Department of Chemical Engineering, Technion – Israel Institute of Technology, Haifa 3200003 Israel
[e] The Nancy & Stephan Grand Technion Energy Program (GTEP), Technion, Israel Institute of Technology, Haifa 3200003, Israel

ARTICLE INFO

Article history:
Received 13 January 2016
Received in revised form
30 March 2016
Accepted 9 April 2016
Available online 14 April 2016

Keywords:
Anion exchange membrane
Quaternary ammonium poly(sulfone)
Counter ions
Anion transport
Ionic diffusion

ABSTRACT

Quaternary ammonium poly(sulfone) based anion exchange membrane (AEM) in Cl^- and HCO_3^- forms were characterized chemically and morphologically. It was found that the surface of the membrane in both of the forms has highly connective island-like structure, where the diameters of the hydrophilic regions are approximately 5–20 nm. Thermal gravimetric analysis of the membrane in the HCO_3^- form presented lower decomposition temperatures for the backbone and the side chains, than the membrane in the Cl^- form. In addition, the AEM in its HCO_3^- form showed higher water uptake values than in its Cl^- form across the temperature range of 25–80 °C. Conductivity experiment measured at same temperatures in both AEM forms showed higher results for Cl^- form than for HCO_3^- form. A computational model was developed in order to understand the conductivity mechanism and the relevant parameters that limit ion transport in these materials. Together with the experimental results, it was found that only 40% of the ions are free for ionic conductivity, while 60% of the ions are bound to the cationic groups, therefore unavailable to participate in the conduction process.

1. Introduction

Recently, there has been growing interest in anion exchange membranes (AEMs) for use in electrochemical systems such as alkaline AEM fuel cells, electrolyzers and water purification devices [1,2]. AEMs generate an alkaline environment internal to the device which gives the opportunity to use platinum free [3] as well as non-precious metal catalysts for electrochemical conversion in these processes [4], substantially reducing the device costs. In addition, AEMs may be compatible with other fuels besides hydrogen [5,6], and thus relevant for a wide family of fuel cell designs.

At present, there are a few obstacles to the use of AEMs including low chemical and thermal stability in alkaline environment [6,7]. Degradation of the chemical structure of both, side chains and the backbone, lead to deteriorated performance and short lifetime of the fuel cell. Another challenge regarding AEMs is their low ionic conductivity [8]. Hydroxide has one-half the dilute solution mobility of protons in aqueous solution, therefore, the low ion mobility is one factor in reduced conductivity of AEMs compared to proton exchange membranes [9]. Other barriers to low conductivity in AEMs are unknown, since the anion conductivity mechanism is being investigated and the complete mechanism in polymer membranes is still not clear [10].

Researchers report that hydroxide transports in AEMs is a combination of Grotthuss mechanism, diffusive transport and hopping mechanisms [11]. The Grotthuss mechanism, which is considered to be the dominant transport mechanism for hydroxide, describes hydroxide transport through AEMs by hydrogen-bonded network of water molecules (Scheme 1a [12]). The movement of the hydroxide ion is accompanied by a hyper-coordinating water molecule. The hydrated hydroxide ion is coordinated to four electron-accepting water molecules [13,14] such that when an incoming electron-donating hydrogen bond forms fully tetrahedral coordinated water molecule may be easily

☆ This work is dedicated to the memory of the late Professor Arnon Siegmann, a dear friend and a colleague at the Technion's Department of Materials Science and Engineering, who passed away on March 2016. Professor Siegman's pioneering work on polymer-ceramic composite materials has a vast and most important impact on the Materials Research community.

* Corresponding author at: Department of Materials Science and Engineering, Technion, Israel Institute of Technology, Haifa 3200003 Israel.
E-mail address: eineli@tx.technion.ac.il (Y. Ein-Eli).

http://dx.doi.org/10.1016/j.memsci.2016.04.027
0376-7388/

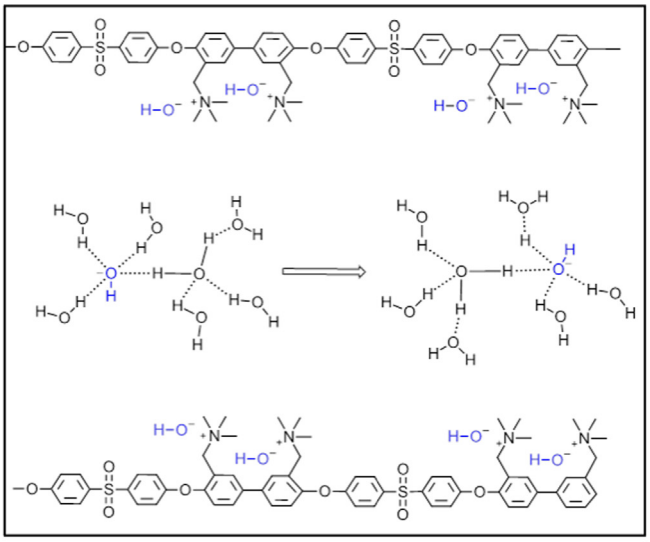

1a. Grotthuss mechanism.

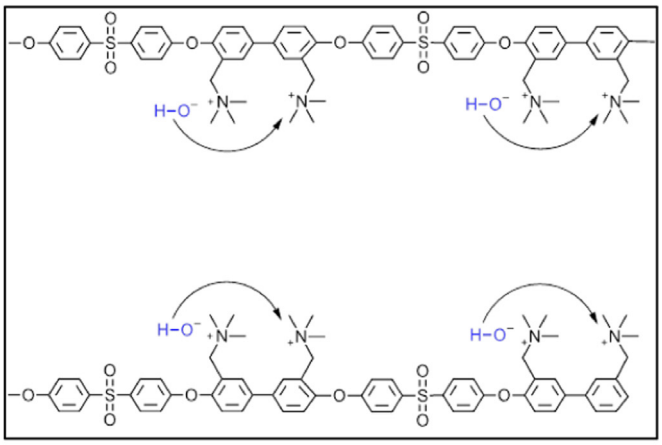

1b. Surface site hopping mechanism.

Scheme 1. a. Grotthuss mechanism. b. Surface site hopping mechanism.

formed. Diffusive transport occurs in the presence of a concentration or electrical potential gradient. Surface site hopping (Scheme 1b), known as vehicular or hopping mechanism, occurs between cationic groups and recognized to be of secondary importance [11].

Investigating hydroxide transport in an alkaline AEM simulating fuel cell conditions is challenging at this stage of knowledge for two main reasons; first, hydroxide form is quickly converted to less conductive CO_3^{-2} and HCO_3^- anion forms when exposed to CO_2 and causes a mix of participate anions [9], leading to confusion in the interpretation of the results. In addition, during the experiment, hydroxide interacts with cationic groups via SN_2 and E_2 reactions [15], reducing the IEC of the membrane, thus changing their inner structure. Low humidity conditions, as present inside fuel cells, are a complex environment for ion conductivity as well. In particular, low humidity leads to partial solvation of ions or to region of non-solvated ions [16], creating a blend of hydrophobic/hydrophilic regions making analysis even more demanding.

Anions inside the membrane can be either ion-paired with the cationic side chains or free ions. Only the free ion may be transport and can therefore contribute to the conductivity. Transport of free ions inside a membrane, and thus conductivity, could be influenced by numerous parameters such as volume of hydrophilic domains through which ions are transported, tortuosity, connectivity, steric effects, degree of ionization and ion size [17]. Phase separation and morphology are known to play key roles in fundamental properties such as ion conductivity and diffusion coefficients within the membranes.

A solution for designing highly conductive membranes is needed to identify which parameter limits the transport in AEMs. Therefore, our approach is to study AEMs in the Cl^- and HCO_3^- forms. These forms are not affected by the presence of CO_2 when the AEM is exposed to the atmosphere, and the membrane is not being chemically degraded by the attack of the anion as in the case of the AEM in the hydroxide form. The investigated counter anions, Cl^- and HCO_3, are transported via en-mass diffusion mechanism, which is well known and understood. In addition, we avoid difficulties that arise due to low humidity condition by focusing on a fully hydrated membrane. Overall, this setting is appropriate for an initial investigation of the influence of the counter ion on the basic membrane properties. The anions differ in size, chaotropic or cosmotropic nature, i.e. the influence of ions on the hydrogen bonds in water molecules, and ion-pairing tendency. These properties will allow us to identify the crucial factors for an efficient ionic transport in AEMs, while it may be even plausible that some of these factors would be relevant to hydroxide ion transport in AEMs.

2. Experimental

2.1. Polymer synthesis

Scheme, 2 shows the chemical structure of a quaternary ammonium (QA) biphenol poly(sulfone)-based AEM synthesized by chloromethylation of a commercially-available Radel polymer backbone. The AEMs in this report were synthesized using previous methods [18].

2.2. HRSEM

The membranes were cut into squares of approximately 5 mm × 5 mm and were fixed onto an aluminum stub with a double-sided conductive tape (for cross-section images, the membrane was freeze-cut). Then, the samples were sputter coated with a carbon, to improve conductivity. The observation was conducted with an acceleration voltage of 4–3 kV in a high-resolution scanning electron microscopy (HRSEM, Zeiss Ultra-Plus FE-SEM).

2.3. Ion exchange capacity (IEC)

Ion exchange capacity was measured using a potentiometric method [19]. This method enhances the accuracy of the Mohr titration method for IEC determination, especially when small quantities are measured. A membrane sample (in Cl^- form) of 30×30 mm^2, with thickness of 0.070–0.10 mm was immersed in 50 mL 0.2 M KNO_3 solution for 24 h (the solution was refreshed 3 times) and titrated with 0.02–0.1 M $AgNO_3$. The IEC was

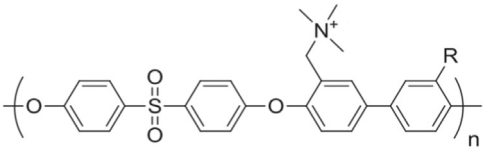

R = H or $CH_2N^+(CH_3)_3OH^-$

Scheme 2. Chemical structures of quaternary ammonium functionalized poly (sulfone) anion exchange membrane.

calculated *via*:

$$\mathrm{IEC} = \frac{\Delta V_{AgNO3}\, C_{AgNO3}}{m_d} \quad (1)$$

where, m_d is the mass of the dry membrane (in the Cl^- form) dried at 60 °C in a vacuum oven for 24 h, ΔV_{AgNO3} is the consumed volume of $AgNO_3$ solution and C_{AgNO3} is the concentration of $AgNO_3$ solution.

2.4. Water uptake

The water uptake in HCO_3^- and Cl^- forms of the membrane was defined as the weight ratio of the absorbed water to that of the dry membrane, as given by:

$$W(\%) = \left(\frac{m_w - m_d}{m_d}\right)\cdot 100\% \quad (2)$$

where, m_d and m_w are the mass of the membrane, before and after water absorption, respectively. The procedure of weighing wet membranes includes surface water elimination by rapid surface drying with a Kimwipe, followed by a drying in a vacuum oven for 24 h at a temperature of 60 °C. The hydration number (see Fig. S1, Supplementary material) was calculated *via*:

$$\lambda = \left(\frac{m_w - m_d}{M_{H_2O}}\right)\cdot\left(\frac{1000}{m_d\cdot \mathrm{IEC}}\right) \quad (3)$$

where, M_{H2O} is the molecular weight of water. All measurements were conducted in triplicate, with three measurements performed on each individual sample [20].

2.5. Dimensional swelling

AEM dimensional swelling was calculated by measuring the film thickness at temperature 25–60 °C, compared with films soaked in water at room temperature for 24 h. Thickness measurements were made (as quickly as possible, to prevent drying) using a digital Mitutoyo micrometer (precision of ±2 μm). Wet membranes were removed from the liquid, and blotted to remove surface water. All measurements were conducted in triplicate, with three thickness measurements performed on each individual sample.

2.6. Conductivity

The ionic conductivity (σ, S cm^{-1}) of HCO_3^- and Cl^- forms of the membranes (size: 10 mm × 20 mm) were measured by two probe in-plane impedance spectroscopy, using $\sigma = d/L_s W_s R$ (d is the distance between reference electrodes, L_s and W_s are the thickness and width of the membrane, respectively). The membrane impedance was measured over the frequency range from 10 kHz to 10 mHz, with an AC amplitude of 10 mV and a 0 mV DC bias, using an PARSTAT 2273 (Princeton Applied Research). The resistance of the membranes was determined from the real part of the impedance at the minimum imaginary value. The measurements were conducted under fully hydrated conditions, with samples being immersed in water at elevated temperatures.

2.7. Thermal gravimetric analysis (TGA)

TGA was used in order to evaluate the short-term thermal properties and stabilities of the samples. The thermal stability of the HCO_3^- and Cl^- forms of the membranes were analyzed using a Q50 TGA (TA Instruments Corporation). Temperature was increased from room temperature to 500 °C at a heating rate of 5 °C min^{-1} in a nitrogen environment.

2.8. Attenuated total reflectance Fourier transformed infra-red spectroscopy (ATR-FTIR)

Spectra (collected after 128 scans with a resolution of 4 cm^{-1}) of the membranes were obtained with the use of a Nicolet iS5 spectrometer equipped with a DTGS detector. A reflection ATR accessory equipped with a diamond crystal at an incident angle of 45° was used. The membrane sample was pressed to the crystal with a clamp-kit to ensure reproducible contact between the sample and the ATR crystal.

2.9. Transport model

The investigated anions, Cl^- and HCO_3^- are transported *via* the en-mass diffusion mechanism, which is well known and understood. We developed a model under the assumption that en-mass diffusion is the only transport mechanism contributing to the conductivity. In this model, conductivity due to en-mass diffusion in bulk water is described by the Nernst-Einstein relation:

$$\sigma_r = \frac{F^2}{RT}\cdot D\cdot C \quad (4)$$

where, D is the diffusion coefficient of the ion in water, C is the ionic concentration per unit of absorbed water, F is the Faraday constant, R is the gas constant, and T is the temperature. We adapted this formula to describe AEM conductivity:

$$\sigma_{AEM} = \frac{F^2}{RT}\cdot D_{eff}\cdot C_{free} \quad (5)$$

here, D_{eff} is an effective diffusion coefficient:

$$D_{eff} = \frac{\upsilon}{\tau}\cdot D \quad (6)$$

where, υ is the volume fraction of pores, and τ is the tortuosity factor. The ionic concentration, C, is directly related to IEC:

$$C = \frac{m_d}{(v_w - v_d)}\cdot IEC \quad (7)$$

where, m_d is the weight of the dry membrane, and v_w, v_d are the volumes of the wet and dry membrane, respectively. Formula (5), however, considers the concentration of free ions, i.e., anions that are not ion-paired with the side-chains and therefore, can be transported:

$$C_{free} = \alpha\cdot C \quad (8)$$

where α is the percent of free ions. The concentration of free ions depends non-linearly on the IEC. Indeed, following ion association thermodynamic theory, see e.g. [21, Section, 3.1] while neglecting confinement effects,α satisfies,

$$K_{as} = \frac{1-\alpha}{\gamma^2\alpha^2 m_e} \quad (9)$$

where, K_{as} is the thermodynamic ion-pair association constant, γ is the mean ionic activity coefficient, and m_e is the molality of the solution which satisfies:

$$m_e = \frac{1}{10}\cdot\frac{m_w\cdot IEC}{m_w - m_d} \quad (10)$$

where, m_w and m_d are the weights of the wet and dry membrane, respectively. Therefore, the overall relation between conductivity and IEC takes the form:

$$\sigma = D_{eff}\cdot\frac{F^2}{RT}\cdot\frac{m_d\cdot\alpha\cdot(IEC)}{(v_w - v_d)}\left(IEC - IEC_0\right) \quad (11)$$

where, IEC_0 is a threshold value for conductivity, closely related to

the percolation threshold of the interconnected hydrophilic domains. In Section 3.7 we apply this model for a computational analysis of experimental data.

3. Results and discussion

3.1. Water uptake

Water uptake measurements show that over a wide range of temperatures, the membrane in HCO_3^- form absorbs more water molecules than the membrane in Cl^- form (see Fig. 1) [22]. These results suggest that the dominant factors that dictate the water absorbance are hydration number, dissociation factor and the coulombic interaction between the counter ion and the cationic group. Indeed, the approximate coordination number of Cl^- in water was found in experimental reports to vary from 4 to 9 and in theoretical studies, from 5.1 to 8.4 [23,24]. However, HCO_3^-has a hydration shell of 7–8 water molecules, higher than Cl^- form, with 3-4 hydrogen bonds formed between the oxygen atoms of the bicarbonate ion and the hydrogen atoms from the solvating water molecules [25]. The dissociation constant of the salt and the ion pairing with the buildup of the hydration shell should be taken into account, as these may have an influence on the water uptake, as well. In our case, $pKb_{KHCO3} < pKb_{KCl}$ therefore, HCO_3^-will dissociate more than Cl^-. Another aspect is the electronegativity of the anions Cl^- and oxygen of HCO_3^-, Cl^- has higher electronegativity values than oxygen in HCO_3^- therefore, will be strongly attracted to the fixed polymer's C_4N^+; thus, it will probably possess mutual ion pair hydration shell, opposed to HCO_3^-. In addition, we observe a steep increase in water uptake at the temperature range of 60–80 °C. It is plausible that this increase is due to a significant structural modification that enables the membrane to absorb more water molecules.

Thickness, being one of the parameters that contribute to the membranes swelling, was measured and is presented in Fig. 2. At room temperature, the thickness increase of Cl^- is 3%, while that of HCO_3^- is 6%. Thickness of HCO_3^- form has higher values than the Cl^- form, in accordance with the membranes water uptake results. Thickness results showed a steep increase from 50 to 80 °C, as was seen already in the water uptake results.

3.2. Morphology

Tapping mode phase images of the surface of the membrane in the Cl^- and HCO_3^- forms, was recorded at temperature of 25 °C, on a 250 nm × 250 nm surface. It is known that the slope of morphological features can contribute to the phase [26]. Thus, in order to overcome this issue, we sampled regions with the lowest possible morphology changes, and in addition, we increased the scale to accommodate a surface of 150 nm × 150 nm square [27]. The dark regions shown in Fig. 3 correspond to the soft hydrophilic QA ionic groups and the bright domains correspond to the hard structures of the polysulfone aromatic backbones. Fig. 3 demonstrates a surface with a cluster/island-like structures [28], where the islands represent the backbone of the membrane, and the surrounding represents the hydrophilic channels. These hydrophilic regions, with approximate diameter of 5–20 nm (see Fig. S2, Supplementary material), are inter-connected, yielding superior ion conducting channels. Clearly, there are no significant visible differences in the hydrophilic/hydrophobic regions between Cl^- and HCO_3^- forms of the membrane.

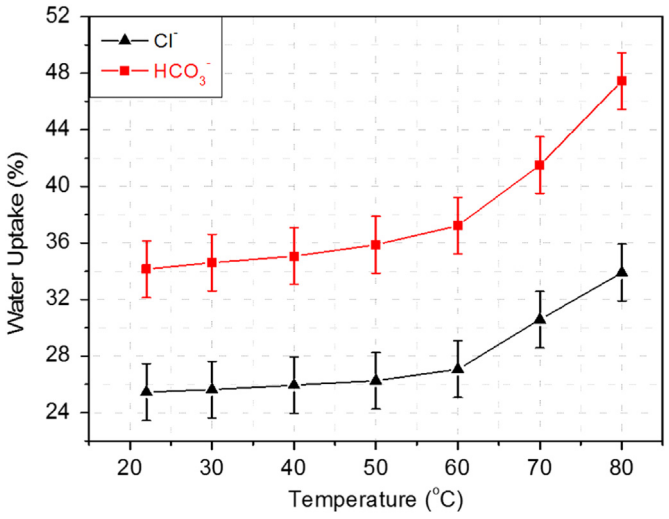

Fig. 1. Water uptake of Cl^- and HCO_3^- forms of the membrane vs. temperature.

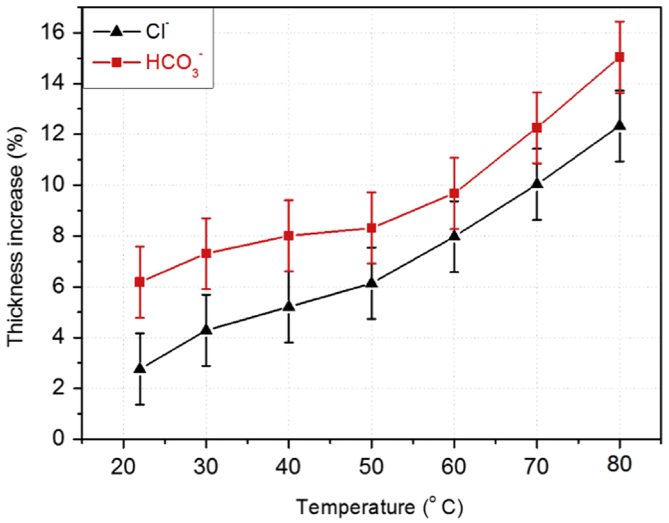

Fig. 2. Thickness increase of Cl^- and HCO_3^- forms of the membrane vs. temperature.

3.3. Conductivity

Fig. 4 displays the results of the conductivity measurements of Cl^- and HCO_3^-forms of the membrane at different temperatures. At room temperature, the average conductivity of Cl^- is 8 mS cm^{-1}, while that of $HCO_3^-$is 6 mS cm^{-1}; the alteration of the conductivity values between the Cl^- and HCO_3^-forms is within the given statistics. Usually, ionic conductivity increases with water sorption, due to conductivity mechanism that involve water molecules, and due to swelling of the hydrophilic domains, through which water and ions are transported. In this case, the conductivity results indicate that the amount of water molecules have a minor influence on the main conductivity mechanism.

There is a fundamental difference in the investigated anions, which is their mass and size, i.e. ion hydration radius. We postulate that the conductivity mechanism, referring to the average conductivity results, is affected by the size of the hydrated ion. Smaller hydrated ions, as Cl^-, move through the hydrophilic domains faster. This would mean that the conductivity should scale inversely with ion-hydrated radius. In addition, it is possible that due to the large size of bicarbonate, its surface electric field is weaker than that of Cl^-, and therefore it does not hold on its solvation water molecules as tightly as Cl^- does and thus, tends to bind more strongly with the QA groups [29,30].

At elevated temperatures, the polymeric backbone, and the side chains will increase theirs flexibility, providing a larger free

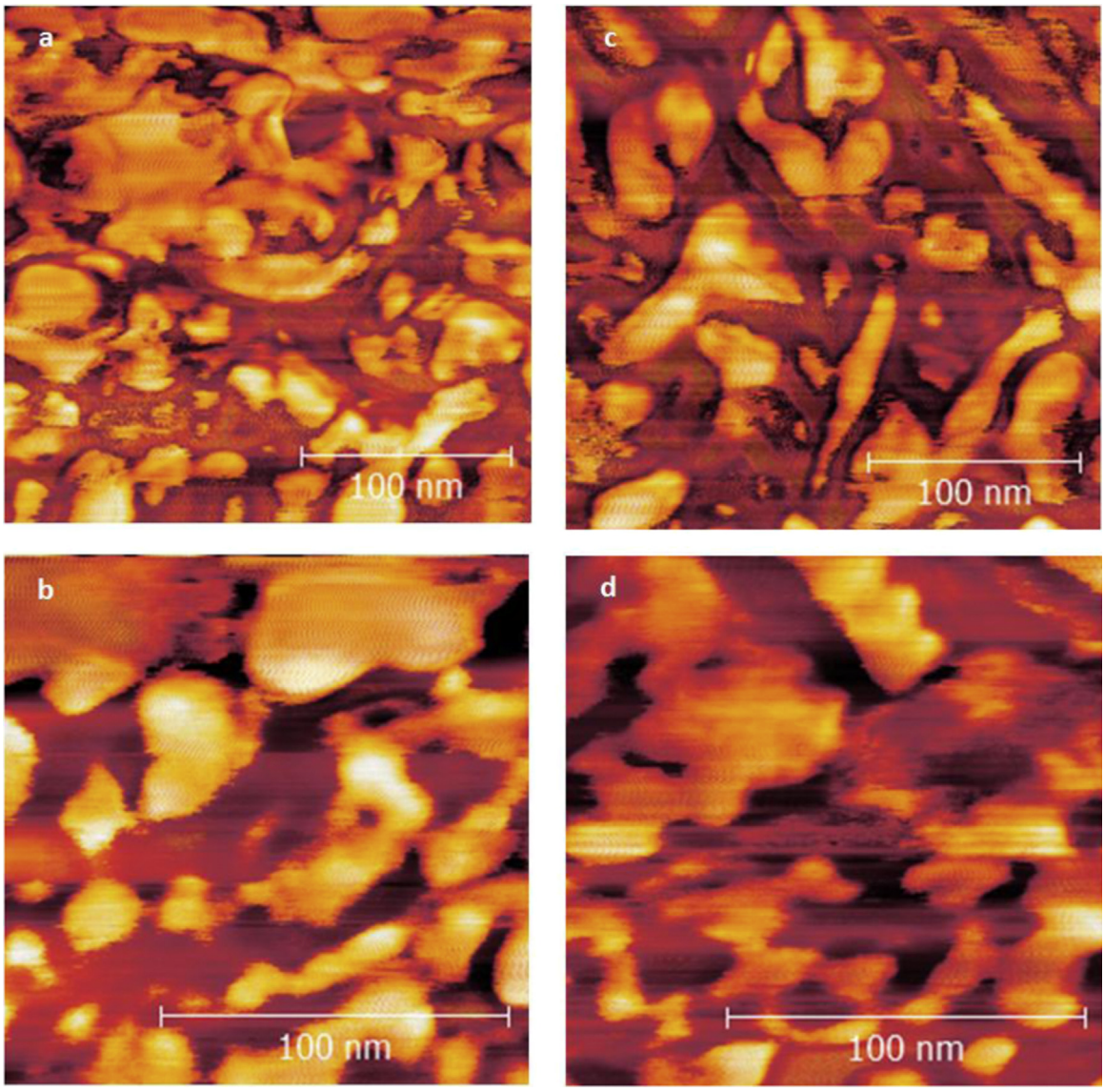

Fig. 3. AFM images of Cl^- (a, b) and HCO_3^- (c, d) forms of the membrane.

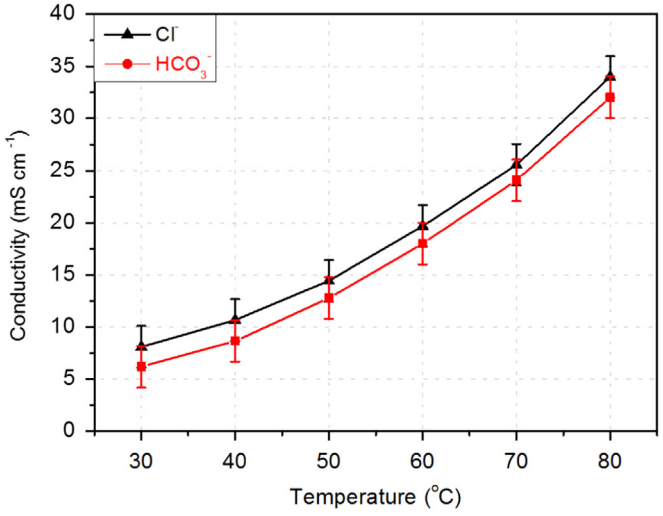

Fig. 4. Conductivity of Cl^- and HCO_3^- forms of the membrane vs. temperature.

volume, leading to higher connectivity in favor of enhanced ion transport [31]. In addition, faster diffusion, more fluctuations and thermal motion of ion would promote the conduction at elevated temperatures, overcoming the activation energy for ion transport. In contrast to the water uptake measurements, we do not observe a steep change in conductivity in the temperature range of 60–80 °C (see Fig. 4). Therefore, the structural changes in the membrane that were hypothesized in the water uptake section (see Section 3.1), does not influence on the dominant conductivity mechanism.

3.4. HRSEM and visual color change

Fig. 5 presents photo images of the flexible, transparent and yellowish hue membrane in Cl^- and HCO_3^- forms. The HCO_3^- form presented more yellowish hue than the Cl^- form. In some cases, yellowish color is attributed to chemical degradation of the membrane [32]; however, this is probably not the case, since the membranes were not exposed to corrosive environment or to any extended light radiation period. Consequently, membrane's color can be a manner of the counter-ion type contribution, as well.

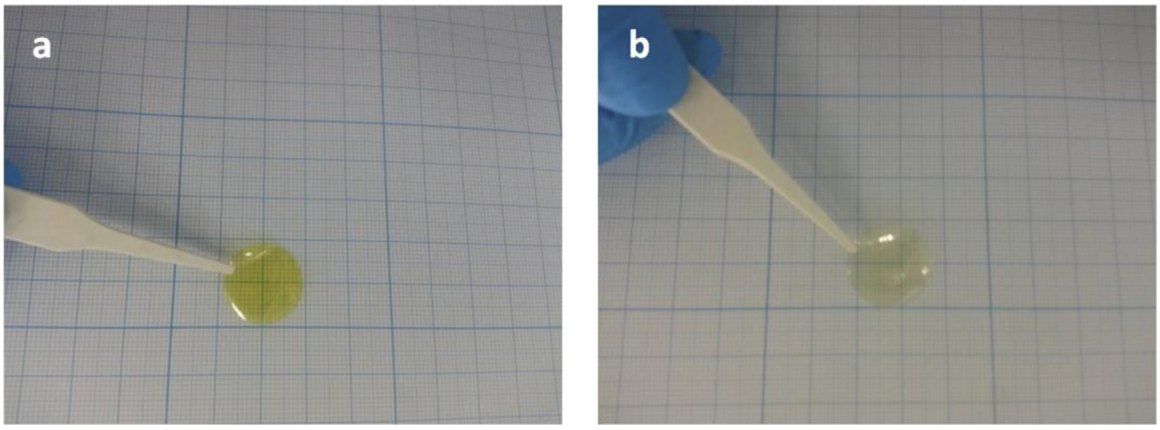

Fig. 5. Photo images the membrane in HCO_3^- (a) and Cl^- (b) forms. (For interpretation of the references to color in this figure, the reader is referred to the web version of this article.)

HRSEM surface morphologies images and cross sectional views of the Cl^- and HCO_3^- forms of the membranes are shown in Fig. 6 left and right columns respectively. No clear or significant difference between the images obtained from the Cl^- and HCO_3^- forms was detected. The surfaces of the membranes are uniform, without any cracks or visible pores. Some lines and pits are observed at the surfaces of the membranes. However, it seems as that these were probably formed during the synthesis process.

The enlarged cross sectional images display a rough layer, represented by circular lumps creating folded cavities to be irregularly distributed. It is reasonable to think that the cavity structure enables the membrane to absorb more water molecules, which may explain the high water uptake results.

3.5. Thermal stability

Assessment of the membranes' thermal stabilities was conducted with the use of TGA. Fig. 7 presents TGA curves of the HCO_3^- and Cl^- forms of the membranes under nitrogen atmosphere recorded from 25 to 550 °C. The decomposition temperature can be determined from derivation of thermogravimetric analysis curve, as can be seen in the inset of Fig. 7. Within this temperature range, three major stages of mass losses were observed [33]. The first step in the HCO_3^- form of membrane was observed at 50 °C and it is probably due to a removal of the weakly bound free water molecules within the membrane. The second major mass loss in the HCO_3^- form of the membrane occurred at 168 °C, and could indicate a decomposition of the bicarbonate groups. The next decomposition step is represented by shallow, broad and overlapping peaks in the temperature range of 195–255 °C. This decomposition step might include a few steps: the first one might be related to HCO_3^- groups, which were strongly bounded to the cationic groups, integrated with the decomposition steps of QA [34]. QA groups could also decompose in a few steps, arising from different degradation mechanisms. The last stage of mass loss was ascribed to the membrane's main chain decomposition, commencing around 413 °C [35]. Three stages for the Cl^- form of membrane are observed as well: the first stage is presumably attributed to water decomposition at 50 °C, the second stage, having a shoulder peak, could be ascribed to a few decomposition steps of QA at 272 °C, and the last stage, at 430 °C, could be attributed to the backbone decomposition [34].

Apparently, the presence of HCO_3^- causes a decrease in the decomposition temperature of QA and the backbone. As HCO_3^- is heated, decomposition to CO_2 and OH^- occurs. The increase in OH^- concentration with increase in temperature would likely accelerate the degradation of the membrane.

3.6. FTIR Studies

FTIR spectral analysis was carried out in order to investigate the structure of HCO_3^- and Cl^- forms of the membrane. Fig. 8 compares FTIR spectrum of the two forms of the membrane (with Cl^- and HCO_3^- ions, respectively). The peaks that are associated only with HCO_3^- vibrations are located at 1355 cm^{-1} and 1310 cm^{-1} for symmetric stretching of CO_2, 1012 cm^{-1} for stretching of COH, and 640 cm^{-1} for CO_2 bend (see Fig. S3, Supplementary material). A considerable difference in the spectra was found in the region of 1360–1430 cm^{-1} (Fig. 8b). Deconvolution of these peaks, shown in Fig. 8c-d, revealed 5 peaks in the Cl^- form and 6 peaks in the HCO_3^- form, these peaks are associated with the bending of CH_2 and CH_3 in the cationic groups [16]. The additional peak in the HCO_3^- form is located at 1377 cm^{-1} and is assigned to CO stretch. This information leads to the conclusion that the ion type, in this case Cl^- and HCO_3^-, has a minor influence on the chemical structure of the membrane.

3.7. Computational Analysis

We analyze the data with the use of a transport model (11) in order to identify the limiting conductivity's factors and their relative magnitude. To extract the dependence of the free charge density on the IEC, we substitute membranes weight measurement, together with tabulated values of association constant and activity coefficient into relation (9). We found that the free charge density depends only weakly on IEC, i.e., $\alpha(\mathrm{IEC}) \approx 0.35$, see Fig. 9.

Therefore, relation (11) implies a nearly linear dependence between the IEC and conductivity:

$$\sigma_{AEM} \approx \alpha \cdot D_{eff} \cdot \frac{F^2}{RT} \cdot \frac{m_d}{(v_w - v_d)} \cdot (IEC - IEC_0) \tag{12}$$

As expected, linear dependence is observed in the experimental settings, as presented in Fig. 10. The effective diffusion coefficient was extracted by considering the slope of the line $\sigma_{\mathrm{AEM}}(IEC)$, extracted using a standard least-squares method, together with experimental measurement of the water uptake (in volume and weight):

$$D_{eff} \approx \frac{RT}{\alpha F^2} \cdot \frac{(v_w - v_d)}{m_d} \sigma_{AEM}(IEC) \tag{13}$$

The volume fraction v, of the water regions inside the membrane is also extracted using these experimental water uptake measurements. Finally, the tortuosity factor τ, is extracted from the tabulated diffusion coefficients of ion at the bulk and the

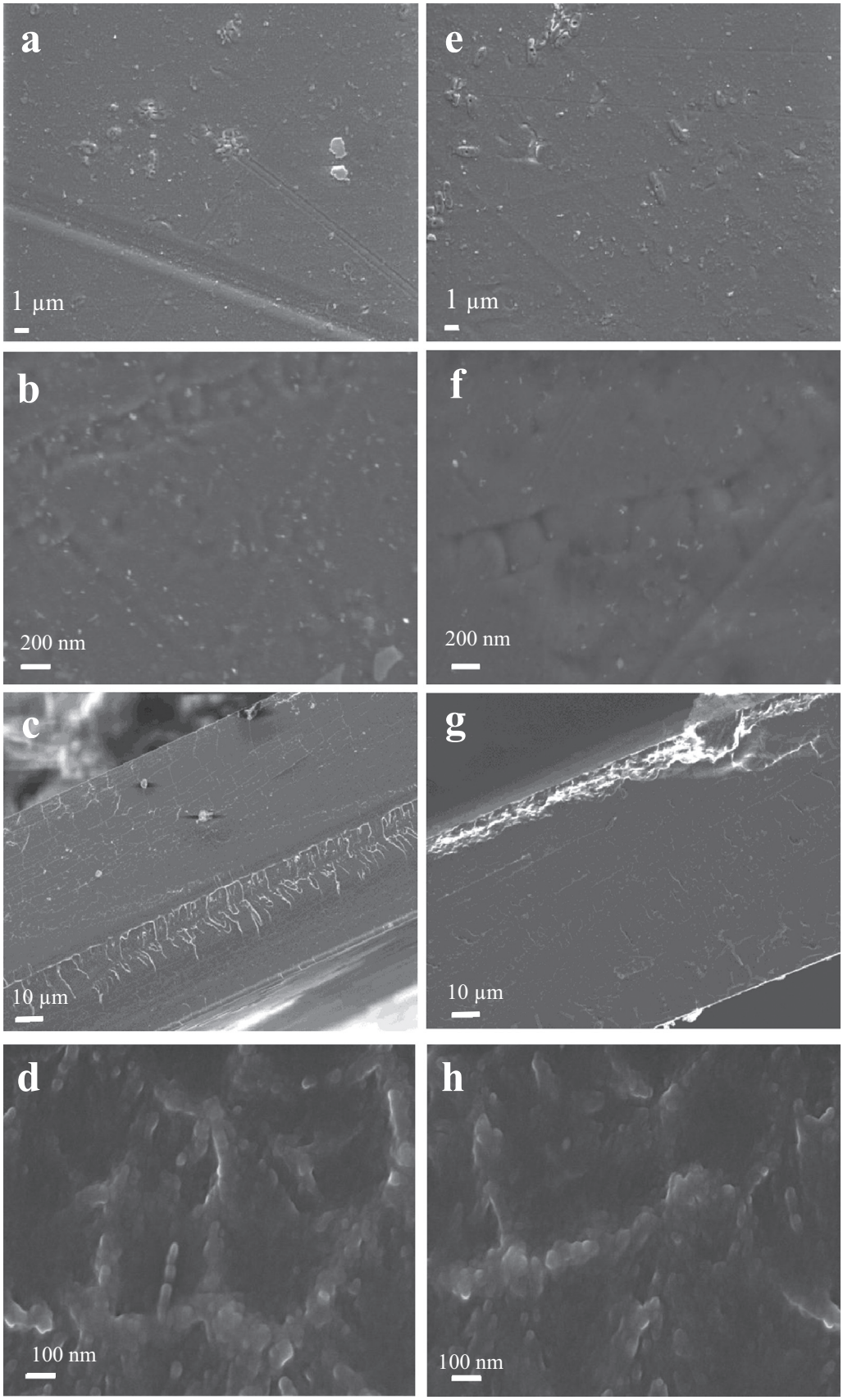

Fig. 6. HRSEM surface (a, b) and cross-section (c, d) images the membrane in Cl^- form. HRSEM surface (e, f) and cross-section (g, h) images the membrane in HCO_3^- form.

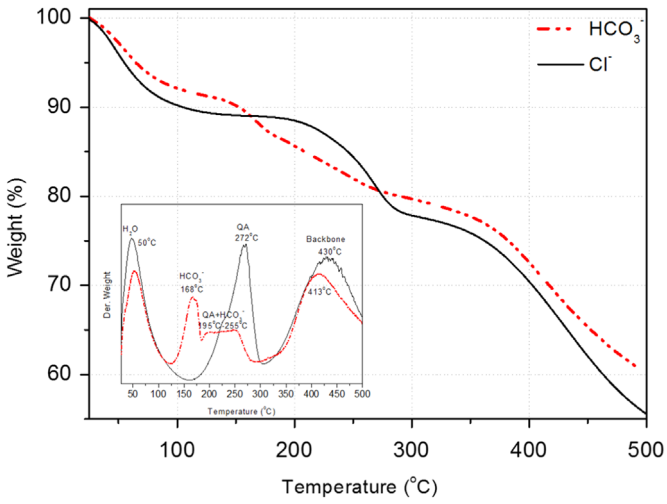

Fig. 7. TGA (DTGA in the inset) curves of HCO_3^- and Cl^- forms of the membrane.

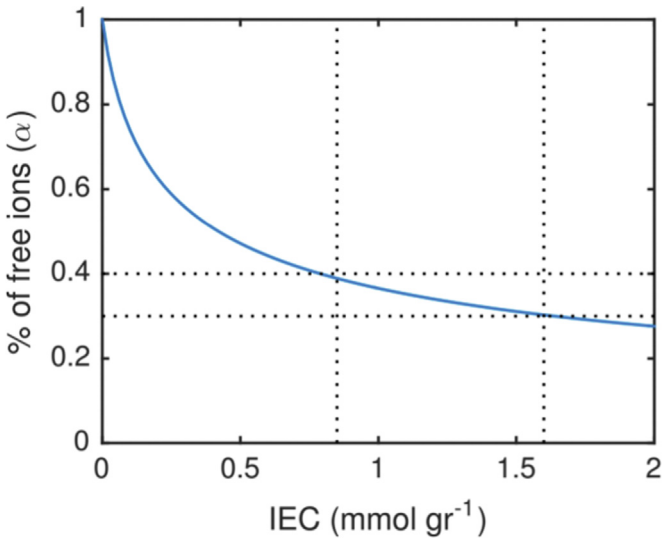

Fig. 9. Percent of free ions, α, as function of IEC for Kas =9.5 and gamma=1 [36] which roughly match experimental data of AEM in Cl^- form. The dotted line marks the region of typical IECs of AEMs. In this range, about 30–40% of the ions are free and contribute to transport.

previously computed values.

$$\tau = \upsilon \cdot \frac{D}{D_{eff}} \tag{14}$$

Our findings (data presented in Table, 1) show that the effective diffusion coefficient in the membrane is roughly 10–14 times smaller than the diffusion coefficients of the anions in bulk water. This could be due to two factors: the volume fraction of the water regions inside the membrane (0.12–0.2) and the tortuosity factor of τ=1.83–1.88.

We conjecture that in HCO_3^- form of the membrane, the effective diffusivity results is over-estimated, since our computation analysis did not account for other ions, such as OH^-, which

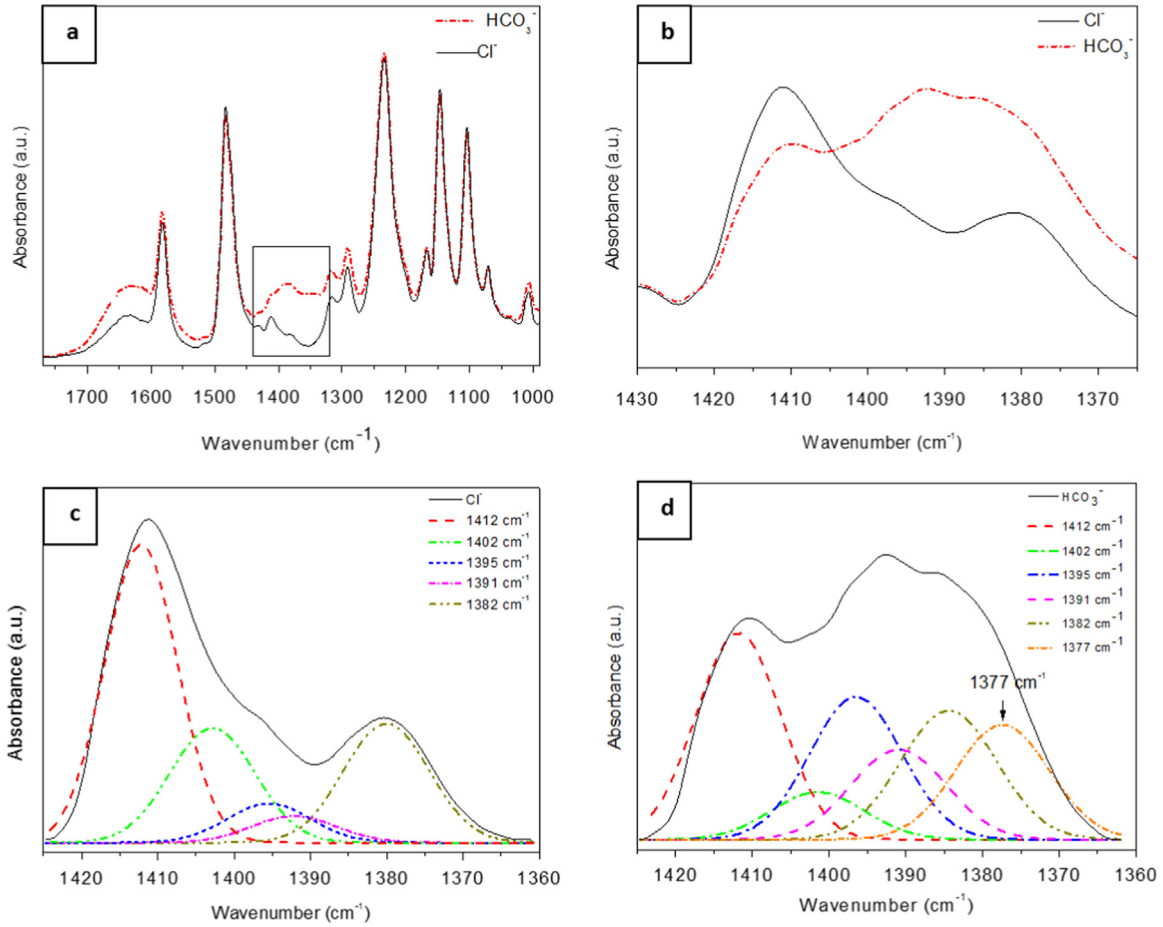

Fig. 8. FTIR spectra of the HCO_3^- and Cl^- forms of the membrane (a); Enlarged FTIR spectra of the 1430–1370 cm^{-1} region of HCO_3^- and Cl^- forms of the membrane (b); Deconvolution of the enlarged FTIR spectra of Cl^- (c) and HCO_3^-(d) forms of the membrane.

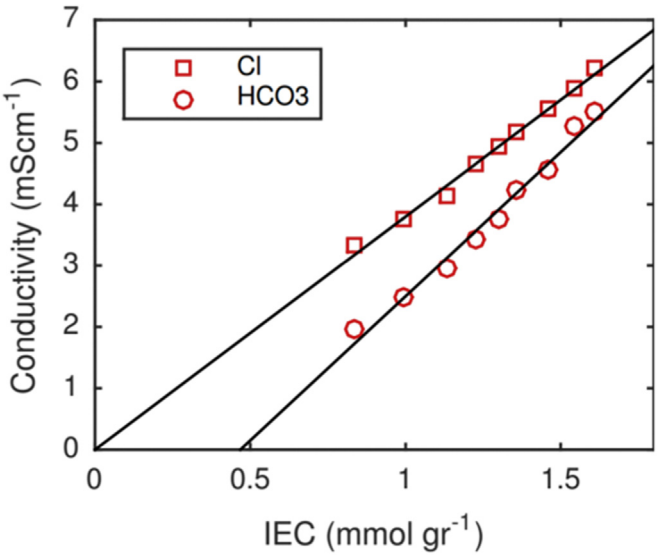

Fig. 10. Experimental data of conductivity and best fitted linear lines for each dataset.

contribute to the conductivity, as HCO_3^- is in equilibrium with some OH^- anions in aqueous solution.

As can be seen in Table 1 and illustrated in Scheme 3 in both Cl^- and HCO_3^- forms of the membrane, about 38–41% of the ions are free, rather than ion-paired with the side-chain, decreasing the conductivity *via* the membrane by an additional factor of ~2.4–2.6.

4. Conclusions

The behavior of quaternary ammonium polysulfone anion exchange membrane in its Cl^- and HCO_3^- forms was investigated. Water uptake measurements showed that the membrane in the HCO_3^- form absorbed more water molecules than in its Cl^- form. AFM measurements, in both of the forms of the membrane, revealed a surface with an island-like structure. This island-like structure is highly inter-connected, yielding superior ion conducting channels. Conductivity measurement showed higher average values for AEM in its Cl^- form than for its HCO_3^- form. The surface of the membranes in both forms is uniform and smooth, while the cross section displayed a rough layer with some shallow folded cavities that can hold water and explain the high water uptake results. TGA measurements showed that the presence of HCO_3^- causes a decrease in the decomposition temperature of QA and the backbone.

By analyzing the computational data, we found that the free charge density weakly depends on the IEC. These results, together with the Nernst-Einstein relation, imply a nearly linear dependence between the IEC and conductivity. The computational analysis reveals the limiting factors for the conductivity and their relative magnitude. In particular, a limited water uptake decreases the conductivity by a factor of 5–8, and an additional factor of 1.83–1.88 is lost, due to the morphological arrangement of the water regions (quantified as the tortuosity factor). Finally, we found that in both Cl^- and HCO_3^- forms of the membrane, ~40% of the ions are free, rather than ion-paired with the side-chain. This, in-turn decreases the conductivity *via* the membrane by an additional factor of ~2.4–2.6. One of the ways to improve the low percentage of the free ions in this case, will be to increase the basicity of the functional groups. Another option will be to add a bulky group to the side chains or, the backbone that will sterically hinder the ion pairing.

Table 1
Transport properties of quaternary ammonium functionalized poly(sulfone) anion exchange membrane.

	Water uptake (weight)	Free ions (%)	τ	υ	D_{AEM}/D	σ_{AEM}/σ
Cl^-	28%	38%	1.88	0.12	0.07	0.026
HCO_3^-	34%	41%	1.83	0.20	0.11	0.045

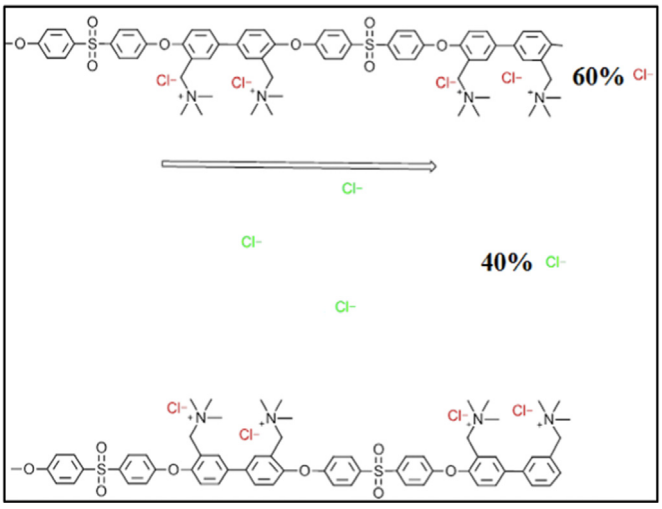

Scheme 3. Around 40% of the ions are free, while 60% are ion-paired with the side chains.

Acknowledgments

This work was supported by the United States-Israel Binational Science Foundation (BSF) through Energy Project No. 2011521, by the Grand Technion Energy Program (GTEP) through NEVET project, by NG VPR Technion fund, by EU Marie-Curie CIG through Grant no. 2018620 and by the Israel Science Foundation INREP project– Israel National Research Center for Electrochemical Propulsion Systems through Grant no. 2792/11.

Appendix A. Supplementary material

Supplementary data associated with this article can be found in the online version at http://dx.doi.org/10.1016/j.memsci.2016.04.027.

References

[1] J.R. Varcoe, P. Atanassov, D.R. Dekel, A.M. Herring, M.A. Hickner, P.A. Kohl, et al., Anion-exchange membranes in electrochemical energy systems, Energy Environ. Sci. 7 (2014) 3135–3191, http://dx.doi.org/10.1039/C4EE01303D.
[2] S. Maurya, S.-H. Shin, Y. Kim, S.-H. Moon, A review on recent developments of anion exchange membranes for fuel cells and redox flow batteries, RSC Adv. 5 (2015) 37206–37230, http://dx.doi.org/10.1039/C5RA04741B.
[3] M. Alesker, M. Page, M. Shviro, Y. Paska, G. Gershinsky, D.R. Dekel, et al., Palladium/nickel bifunctional electrocatalyst for hydrogen oxidation reaction in alkaline membrane fuel cell, J. Power Sources 304 (2015) 332–339, http://dx.doi.org/10.1016/j.jpowsour.2015.11.026.
[4] Q. He, X. Yang, R. He, A. Bueno-López, H. Miller, X. Ren, et al., Electrochemical and spectroscopic study of novel Cu and Fe-based catalysts for oxygen reduction in alkaline media, J. Power Sources 213 (2012) 169–179, http://dx.doi.org/10.1016/j.jpowsour.2012.04.029.
[5] Y. Zhang, J. Fang, Y. Wu, H. Xu, X. Chi, W. Li, et al., Novel fluoropolymer anion exchange membranes for alkaline direct methanol fuel cells, J. Colloid

Interface Sci. 381 (2012) 59–66, http://dx.doi.org/10.1016/j.jcis.2012.05.043.
[6] S. Shiraishi, Encycl. Appl. Electrochem. (2014), http://dx.doi.org/10.1007/978-1-4419-6996-5.
[7] a Amel, L. Zhu, M. Hickner, Y. Ein-Eli, Influence of sulfone linkage on the stability of aromatic quaternary ammonium polymers for alkaline fuel cells, J. Electrochem. Soc. 161 (2014) F615–F621, http://dx.doi.org/10.1149/2.044405jes.
[8] M.R. Hibbs, M.A. Hickner, T.M. Alam, S.K. McIntyre, C.H. Fujimoto, C. J. Cornelius, Transport properties of hydroxide and proton conducting membranes, Chem. Mater. 20 (2008) 2566–2573, http://dx.doi.org/10.1021/cm703263n.
[9] J. Yan, M.A. Hickner, Anion exchange membranes by bromination of benzylmethyl-containing poly(sulfone)s, Macromolecules 43 (2010) 2349–2356, http://dx.doi.org/10.1021/ma902430y.
[10] M.E. Tuckerman, D. Marx, M. Parrinello, The nature and transport mechanism of hydrated hydroxide ions in aqueous solution, Nature 417 (2002) 925–929, http://dx.doi.org/10.1038/nature00797.
[11] K.N. Grew, W.K.S. Chiu, A. Dusty Fluid, Model for predicting hydroxyl anion conductivity in alkaline anion exchange membranes, J. Electrochem. Soc. 157 (2010) B327, http://dx.doi.org/10.1149/1.3273200.
[12] H. Takaba, N. Shimizu, T. Hisabe, K. Alam, Modeling of transport mechanisms of OH - in electrolyte of alkaline fuel cell, ECS Trans. 61 (2014) 63–69, http://dx.doi.org/10.1149/06113.0063ecst.
[13] J.S. Hub, M.G. Wolf, C. Caleman, P.J. van Maaren, G. Groenhof, D. van der Spoel, Thermodynamics of hydronium and hydroxide surface solvation, Chem. Sci. 5 (2014) 1745–1749, http://dx.doi.org/10.1039/c3sc52862f.
[14] T. Megyes, S. Bálint, T. Grósz, T. Radnai, I. Bakó, P. Sipos, The structure of aqueous sodium hydroxide solutions: a combined solution x-ray diffraction and simulation study, J. Chem. Phys. 128 (2008) 1–12, http://dx.doi.org/10.1063/1.2821956.
[15] S. Chempath, B.R. Einsla, L.R. Pratt, C.S. Macomber, J.M. Boncella, J.A. Rau, et al., Mechanism of tetraalkylammonium headgroup degradation in alkaline fuel cell membranes, J. Phys. Chem. C. 112 (2008) 3179–3182, http://dx.doi.org/10.1021/jp7115577.
[16] T.P. Pandey, A.M. Maes, H.N. Sarode, B.D. Peters, S. Lavina, K. Vezzù, et al., Interplay between water uptake, ion interactions, and conductivity in an e-beam grafted poly(ethylene-co-tetrafluoroethylene) anion exchange membrane, Phys. Chem. Chem. Phys. 17 (2015) 4367–4378, http://dx.doi.org/10.1039/C4CP05755D.
[17] X. Yan, G. He, X. Wu, J. Benziger, Ion and water transport in functionalized PEEK membranes, J. Memb. Sci. 429 (2013) 13–22, http://dx.doi.org/10.1016/j.memsci.2012.11.026.
[18] J. Yan, H.D. Moore, M.R. Hibbs, M.A. Hickner, Synthesis and structure-property relationships of poly(sulfone)s for anion exchange membranes, J. Polym. Sci. Part B Polym. Phys. 51 (2013) 1790–1798, http://dx.doi.org/10.1002/polb.23331.
[19] F. Karas, J. Hnát, M. Paidar, J. Schauer, K. Bouzek, Determination of the ion-exchange capacity of anion-selective membranes, Int. J. Hydrog. Energy 39 (2014) 5054–5062, http://dx.doi.org/10.1016/j.ijhydene.2014.01.074.
[20] R.C.T. Slade, J.R. Varcoe, Investigations of conductivity in FEP-based radiation-grafted alkaline anion-exchange membranes, Solid State Ion. 176 (2005) 585–597, http://dx.doi.org/10.1016/j.ssi.2004.09.044.
[21] W.R. Fawcett, Liquids, Solutions, and Interfaces: From Classical Macroscopic Descriptions to Modern Microscopic Details, 2004.
[22] M.L. Disabb-Miller, Z.D. Johnson, M. a Hickner, Ion motion in anion and proton-conducting triblock copolymers, Macromolecules 46 (2013) 949–956, http://dx.doi.org/10.1021/ma301947t.
[23] A. Tongraar, J. T-Thienprasert, S. Rujirawat, S. Limpijumnong, Structure of the hydrated Ca(2+) and Cl(−): combined X-ray absorption measurements and QM/MM MD simulations study, Phys. Chem. Chem. Phys. 12 (2010) 10876–10887, http://dx.doi.org/10.1039/c0cp00136h.
[24] A. Tongraar, B. Michael Rode, The hydration structures of F??? and Cl??? investigated by ab initio QM/MM molecular dynamics simulations, Phys. Chem. Chem. Phys. 5 (2003) 357–362, http://dx.doi.org/10.1039/b209240a.
[25] J.R. Rustad, S.L. Nelmes, V.E. Jackson, D.A. Dixon, Quantum-chemical calculations of carbon-isotope fractionation in CO2(g), aqueous carbonate species, and carbonate minerals, J. Phys. Chem. A 112 (2008) 542–555, http://dx.doi.org/10.1021/jp076103m.
[26] R. García, Dynamic atomic force microscopy methods, Surf. Sci. Rep. (2002), http://dx.doi.org/10.1016/S0167-5729(02)00077-8.
[27] Y. Liu, J. Wang, Y. Yang, T.M. Brenner, S. Seifert, Y. Yan, et al., Anion transport in a chemically stable, sterically bulky α-C modified imidazolium functionalized anion exchange membrane, J. Phys. Chem. C 118 (2014) 15136–15145, http://dx.doi.org/10.1021/jp5027674.
[28] S.S. He, C.W. Frank, Facilitating hydroxide transport in anion exchange membranes via hydrophilic grafts, J. Mater. Chem. A 2 (2014) 16489–16497, http://dx.doi.org/10.1039/C4TA02942A.
[29] Y.-L.S. Tse, H.N. Sarode, G.E. Lindberg, T.A. Witten, Y. Yang, A.M. Herring, et al., Chloride enhances fluoride mobility in anion exchange membrane/polycationic systems, J. Phys. Chem. C 118 (2013) 845–853, http://dx.doi.org/10.1021/jp409728a.
[30] Y.-L.S. Tse, G.A. Voth, T.A. Witten, Ion mixing, hydration, and transport in aqueous ionic systems, J. Chem. Phys. 142 (2015) 184905, http://dx.doi.org/10.1063/1.4921044.
[31] H. Zarrin, J. Wu, M. Fowler, Z. Chen, High durable PEK-based anion exchange membrane for elevated temperature alkaline fuel cells, J. Memb. Sci. 394–395 (2012) 193–201, http://dx.doi.org/10.1016/j.memsci.2011.12.041.
[32] A. Amel, S.B. Smedley, D.R. Dekel, M.A. Hickner, Y. Ein-Eli, Characterization and chemical stability of anion exchange membranes cross-linked with polar electron-donating linkers, J. Electrochem. Soc. 162 (2015) F1047–F1055, http://dx.doi.org/10.1149/2.0891509jes.
[33] D. Chen, M.A. Hickner, Degradation of imidazolium- and quaternary ammonium- functionalized poly (fluorenyl ether ketone sulfone) anion exchange membranes, ACS Appl. Mater. Interfaces (2012).
[34] M. Tanaka, M. Koike, K. Miyatake, M. Watanabe, Synthesis and properties of anion conductive ionomers containing fluorenyl groups for alkaline fuel cell applications, Polym. Chem. 2 (2011) 99, http://dx.doi.org/10.1039/c0py00238k.
[35] K. Shen, J. Pang, S. Feng, Y. Wang, Z. Jiang, Synthesis and properties of a novel poly(aryl ether ketone)s with quaternary ammonium pendant groups for anion exchange membranes, J. Memb. Sci. 440 (2013) 20–28, http://dx.doi.org/10.1016/j.memsci.2013.02.046.
[36] M. Maeda, H. Furuhashi, J. Ikami, Evaluation of dissociation constants of ammonium ions in aqueous ammonium chloride and potassium chloride solutions and of pertinent higher-order parameters according to the Pitzer approach, J. Chem. Soc. Faraday Trans. 89 (1993) 3371–3374, http://dx.doi.org/10.1039/FT9938903371.